CHARACTERIZATION OF TROPICAL RAINFOREST FOR X-BAND SPACEBORNE SAR CALIBRATION USING TANDEM-X DATA

Luca Dell'Amore[1], *José-Luis Bueso-Bello*[1], *Patrick Klenk*[1], *Jens Reimann*[1], *Paola Rizzoli*[1]

[1]German Aerospace Center (DLR), Microwaves and Radar Institute, Germany

ABSTRACT

Tropical rainforests have been established by the SAR community as well-known calibration sites for the estimation and monitoring of the radar antenna pattern shape in elevation. Here, according to the hypothesis of isotropic scattering, the backscattering coefficient in terms of unit area perpendicular to the antenna, called gamma nought, is assumed to remain constant with respect to the incidence angle. Nevertheless, several studies using X- and C-band sensors have shown a slight dependency of the rainforest backscatter on the incidence angle, as well as on the ground target properties and meteorological conditions. The aim of this work is to present a statistical characterization of radar backscatter at X-band over the equatorial Amazon rainforest using TanDEM-X data, and to provide insights on how to best utilize radar backscatter data in this region for SAR calibration and modelling purposes.

***Index Terms*—** Synthetic Aperture Radar (SAR), SAR Calibration, Amazon Rainforest, TanDEM-X.

1. INTRODUCTION

The radiometric calibration of spaceborne SAR products plays a key role for ensuring a good performance of the whole end-to-end system and requires a precise knowledge of both the radar system and the illuminated target [1, 2]. For example, the shape of the antenna pattern in elevation can be directly estimated by analyzing SAR detected images in presence of a homogeneous backscatter profile in the slant range dimension. This is accomplished by acquiring SAR data over homogeneous distributed targets, under the assumption of isotropic scattering. This is the case of tropical rainforests, such as the Amazon and Congo forests, which have been established by the SAR community as well-known test sites for SAR calibration [3–7], thanks to their homogeneous and almost isotropic signature.

Nevertheless, several studies conducted in C-band, e.g. using the ASCAT C-band scatterometer [8] and the RADARSAT-2 C-band SAR sensor [9], and in X-band with the TanDEM-X mission [10], have shown a slight dependency of the backscatter on the incidence angle as well as on ground target properties and meteorological conditions [11–13].

Typically, the quantity used for measuring and analyzing backscatter levels in SAR data over rainforests is the backscattering coefficient gamma nought $\gamma^0(\theta_l)$, which can be expressed as:

$$\gamma^0(\theta_l) = \beta^0(\theta)\tan\theta_l, \tag{1}$$

being $\beta^0(\theta)$ the radar brightness, θ the slant range-dependent incidence angle, which monotonically increases from near to far range and θ_l the local incidence angle. A precise knowledge of the underlying topography is required in order to precisely estimate the local incidence angle as $\theta_l = \theta - \alpha$, with α being the local terrain slope in the slant range direction. Under the assumption of isotropic scattering, the γ^0 profile over the local incidence angle should be flat.

In this paper we present a characterization of the radar backscatter at X-band over the Amazon rainforest using TanDEM-X data at large scale. In particular, we concentrate on the backscatter dependency on the day time of acquisition and orbit direction, whereby ascending and descending orbit acquisitions are generally acquired in the morning and in the evening, respectively. Moreover, we analyze the seasonal variability of the radar backscatter, concentrating on dry and wet seasons.

2. THE AMAZON RAINFOREST DATA SET

The vast majority of TanDEM-X acquisitions has been acquired using HH polarization, i.e. horizontal polarization in transmit as well as in receive. Overall, we processed 1998 detected SAR images, acquired in StripMap mode in HH channel, at almost-full resolution, i.e. 6 m x 6 m, using the experimental TanDEM-X interferometric processor (TAXI) [14]. We absolutely calibrated each image in order to retrieve β^0 and we generated the corresponding local incidence angle map θ_l using the TanDEM-X global edited DEM [15] and the annotated satellite orbit position. Afterwards, we computed γ^0 by applying eq. (1). Both γ^0 and θ_l are then geocoded and interpolated on a common latitude/longitude grid in order to generate large-scale mosaics. Unlike previous works concerning TanDEM-X backscatter analysis [10, 16], which made use of quicklook images at 50 m resolution [17] in order to limit the computational burden

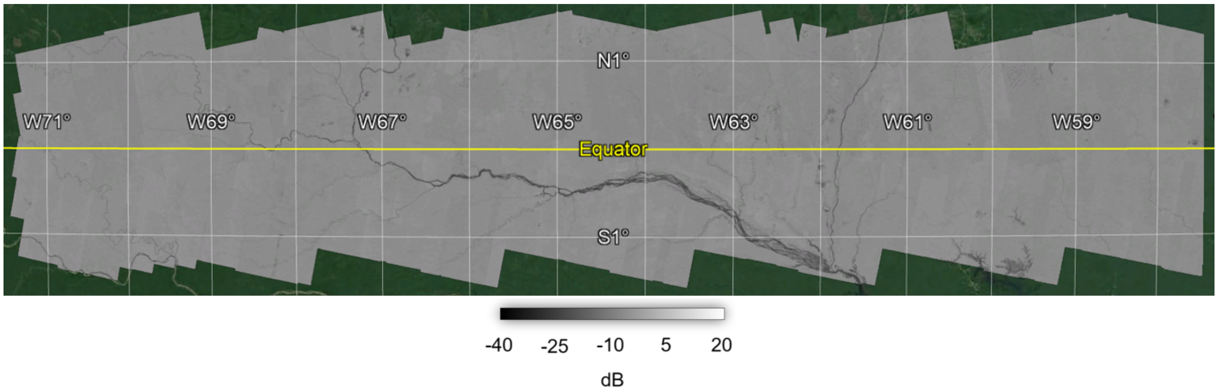

Fig. 1: γ^0 mosaic over the equatorial Amazon rainforest, visualized in GoogleEarth.

when considering large data sets, the present investigation relies on the use of high-resolution data, which allow for a reliable estimation of the complete signal dynamics as explained in [10].

In the following analysis, we focus on the equatorial Amazon rainforest between $[-71°, -58°]$ longitude and $[-1.5°, 1.5°]$ latitude, which comprises images acquired using all twenty nominal TanDEM-X beams used for the generation of the global DEM [18, 19]. Here, we characterize the backscatter dependency on orbit direction and seasonality utilizing the full data set of stripmap, HH polarization data acquired from December 2010 to September 2014. The area is depicted in Fig. 1.

3. γ^0 ANGULAR DEPENDENCY

In this section, we present a large-scale analysis by characterizing the γ^0 radar backscatter at X-band with respect to the local incidence angle θ_l. The full span of nominal local incidence angles θ_l, which span from near (about 25°) to far range (about 51°), has been sampled with angular intervals of 1°. γ^0 samples which belong to each single interval are then grouped together, allowing for the derivation of distribution statistics. Moreover, we applied the TanDEM-X Forest/Non-Forest (FNF) map [20] in order to select the forest pixels only. Given the very different resolution of the FNF map (50 m $\times$ 50 m) compared to γ^0 backscatter data, we eroded forested areas with a square kernel of 5 x 5 pixels, in order to avoid misclassification at the borders. For each incidence angle interval, possible outliers have been then removed by taking only the backscatter distribution between the 1^{st} and 99^{th} percentiles.

The obtained results are presented in Fig. 2 for both data acquired in the morning, i.e. ascending orbit acquisitions, and in the evening, i.e. descending orbit ones. The boxes extend from the lower to upper quartile values of the data distribution, i.e. from the 25^{th} to 75^{th} percentiles, with whiskers

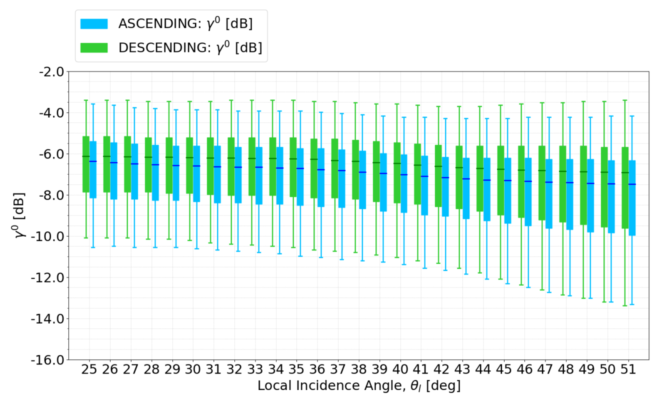

Fig. 2: γ^0 backscatter dependence on local incidence angle. Data distributions are shown for both data acquired in the morning, i.e. ascending orbit acquisitions, and in the evening, i.e. descending orbit ones.

reaching the 5^{th} and 95^{th} percentiles. The solid lines within each box identify the distribution mean value. Here, it is important to mention that all the statistics are computed in linear scale and only afterwards converted to dB. The figure demonstrates the non-fully-isotropic nature of the Amazon rainforest, as the backscatter profiles are not completely flat over the full range of incidence angles. Moreover, ascending and descending orbit acquisitions show a different behavior: acquisitions performed in the morning present lower backscatter values, with a bias of about 0.5 dB, when compared to the ones acquired in the evening. This could be explained by a dependency of the X-band γ^0 backscatter on the level of humidity in the air [13, 21], which can be related to the day-time.

4. γ^0 SEASONAL VARIABILITY

A characterization of the seasonal variability of the radar backscatter over the equatorial Amazon rainforest is presented in the following, by comparing dry and wet seasons.

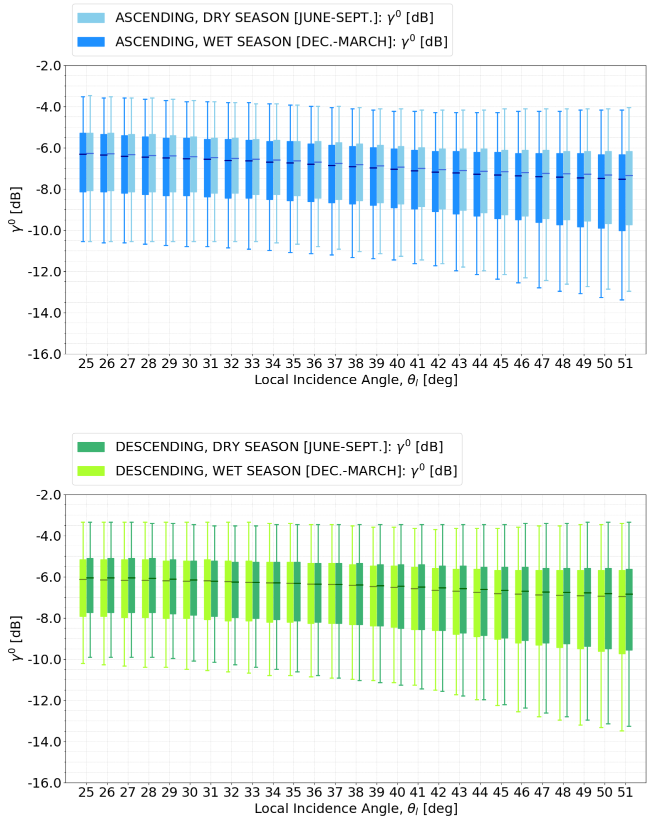

Fig. 3: Seasonal variability of the γ^0 radar backscatter with respect to local incidence angles, by comparing dry and wet seasons. Data distributions are shown for both ascending (top) and descending (bottom) orbit acquisitions.

The statistical analysis relies on the same procedure described in Section 3 and is performed for ascending and descending orbit acquisitions, separately. The two derived data sets are then sub-sampled by considering data acquired during dry and wet seasons, only. For this scope, we assume as dry the months between June and September, while wet acquisitions are collected starting from December till March.
Fig. 3 shows the resultant γ^0 seasonal variability, with respect to local incidence angles. The analysis confirms that no significant difference between the two seasons behavior is detectable. Whereas, it is worth noting that the main driver of the γ^0 radar backscatter over the Amazon rainforest seems to be the day-time of acquisition, as an overall offset of about 0.5 dB can still be seen between ascending and descending orbit data.

5. CONCLUSIONS

In this paper, we presented a statistical characterization of γ^0 radar backscatter at X-band over the equatorial Amazon rainforest using TanDEM-X detected data. Despite the Amazon rainforest appears to be a quite stable and isotropic target, analyses demonstrated its non-fully-isotropic nature, as backscatter profiles slightly decrease with respect to local incidence angles. Moreover, γ^0 properties are influenced by the day time of acquisition, where images acquired in the morning, i.e. in ascending orbit direction, present lower backscatter values, with a bias of about 0.5 dB, when compared to the ones acquired in the evening, i.e. in a descending orbit geometry. We also provided a statistical characterization of γ^0 backscatter depending on seasonality, by comparing dry and wet seasons. In this case, we did not observe significant difference between the two seasons behavior. The work provides useful insights on the properties of SAR distributed scattering mechanisms in the Amazonas, showing different behaviours depending on the day time of acquisition. This information can guide users in a proper exploitation of the area for, e.g., SAR calibration purposes or for the monitoring of the radar antenna pattern. A series of X-band backscatter models for the investigated scenarios are being derived, based on the analyzed TanDEM-X data. To this aim, we rely on the same formulation introduced by Ulaby and Dobson in [22]. The proposed parametric models will be presented at the conference and could then be used for a variety of applications, ranging from SAR system design to physical modelling.

6. REFERENCES

[1] Marco Schwerdt, Benjamin Brautigam, Markus Bachmann, BjÖrn Doring, Dirk Schrank, and Jaime Hueso Gonzalez, "Final terrasar-x calibration results based on novel efficient methods," *IEEE Transactions on Geoscience and Remote Sensing*, vol. 48, no. 2, pp. 677–689, 2009.

[2] Marco Schwerdt, Kersten Schmidt, Núria Tous Ramon, Patrick Klenk, Nestor Yague-Martinez, Pau Prats-Iraola, Manfred Zink, and Dirk Geudtner, "Independent system calibration of sentinel-1b," *Remote Sensing*, vol. 9, no. 6, pp. 511, 2017.

[3] M. Shimada and A. Freeman, "A technique for measurement of spaceborne SAR antenna patterns using distributed targets," *IEEE Transactions on Geoscience and Remote Sensing*, vol. 33, no. 1, pp. 100–114, 1995.

[4] J.L. Alvarez-Perez, M. Schwerdt, and M. Bachmann, "TerraSAR-X antenna pattern estimation by a complex treatment of rain forest measurements," in *2006 IEEE International Symposium on Geoscience and Remote Sensing*. IEEE, 2006, pp. 3857–3860.

[5] M. Bachmann, M. Schwerdt, and B. Brautigam, "TerraSAR-X Antenna Calibration and Monitoring Based on a Precise Antenna Model," *IEEE Transactions on Geoscience and Remote Sensing*, vol. 48, no. 2, pp. 690–701, 2010.

[6] R Hawkins, E Attema, R Crapolicchio, P Lecomte, Josep Closa, PJ Meadows, and SK Srivastava, "Stability of amazon backscatter at c-band: Spaceborne results from ers-1/2 and radarsat-1.," in *SAR workshop: CEOS Committee on Earth Observation Satellites*, 2000, vol. 450, p. 99.

[7] Marco Schwerdt, Kersten Schmidt, Patrick Klenk, Núria Tous Ramon, Daniel Rudolf, Sebastian Raab, Klaus Weidenhaupt, Jens Reimann, and Manfred Zink, "Radiometric performance of the terrasar-x mission over more than ten years of operation," *Remote Sensing*, vol. 10, no. 5, pp. 754, 2018.

[8] Z. Bartalis, W. Wagner, V. Naeimi, D. Sabel, and C. Pathe, "SAR calibration requirements for soil moisture estimation," in *CEOS SAR Calibration and Validation Workshop*, November 2009, Pasadena, California, USA.

[9] S. Cote, S. Srivastava, S. Muir, and T. Lukowsk, "Assessment of distributed target sites within the RADARSAT program," in *CEOS SAR Calibration and Validation Workshop*, November 2011, Fairbanks, Alaska(USA).

[10] P. Rizzoli, B. Bräutigam, and M. Zink, "TanDEM-X large-scale study of tropical rainforests for spaceborne SAR calibration in X-band," in *EUSAR 2014; 10th European Conference on Synthetic Aperture Radar*. VDE, 2014, pp. 1–4.

[11] M. Schwerdt, J. Hueso Gonzalez, M. Bachmann, and D. Schrank, "In-orbit calibration of the TanDEM-X system," in *2011 IEEE International Geoscience and Remote Sensing Symposium*. IEEE, 2011, pp. 2420–2423.

[12] H. Woodhouse, J. van der Sanden, and D. Hoekman, "Scatterometer observations of seasonal backscatter variation over tropical rain forest," *IEEE transactions on geoscience and remote sensing*, vol. 37, no. 2, pp. 859–861, 1999.

[13] Andreas Danklmayer, Björn J Doring, Marco Schwerdt, and Madhu Chandra, "Assessment of atmospheric propagation effects in sar images," *IEEE Transactions on Geoscience and Remote Sensing*, vol. 47, no. 10, pp. 3507–3518, 2009.

[14] P. Prats, M. Rodriguez-Cassola, L. Marotti, M. Nannini, S. Wollstadt, D. Schulze, N. Tous-Ramon, M. Younis, G. Krieger, and A. Reigber, "TAXI: A Versatile Processing Chain for Experimental TanDEM-X Product Evaluation," *Proceedings of the IEEE Geoscience and Remote Sensing Symposium (IGARSS)*, pp. 1–4, 2010.

[15] C. Gonzalez, M. Bachmann, J.L. Bueso-Bello, P. Rizzoli, and M. Zink, "A fully automatic algorithm for editing the TanDEM-X global DEM," *Remote Sensing*, vol. 12, no. 23, pp. 3961, Dec 2020.

[16] P. Rizzoli, M. Martone, and B. Bräutigam, "Global interferometric coherence maps from TanDEM-X quicklook data," *IEEE Geoscience and Remote Sensing Letters*, vol. 11, no. 11, pp. 1861–1865, 2014.

[17] Thomas Fritz, Cristian Rossi, Nestor Yague-Martinez, Fernando Rodriguez-Gonzalez, Marie Lachaise, and Helko Breit, "Interferometric processing of TanDEM-X data," in *2011 IEEE International Geoscience and Remote Sensing Symposium*. IEEE, 2011, pp. 2428–2431.

[18] G. Krieger, A. Moreira, H. Fiedler, I. Hajnsek, M. Werner, M. Younis, and M. Zink, "TanDEM-X: A Satellite Formation for High-Resolution SAR Interferometry," *IEEE Transactions on Geoscience and Remote Sensing*, vol. 45, no. 11, pp. 3317–3341, 2007.

[19] "TanDEM-X ground segment - experimental product description," *DLR public document TD-GS-PS-3028*, January 2012.

[20] M. Martone, P. Rizzoli, C. Wecklich, C. González, J. L. Bueso-Bello, P. Valdo, D. Schulze, M. Zink, G. Krieger, and A. Moreira, "The global forest/non-forest map from TanDEM-X interferometric SAR data," *Remote sensing of environment*, vol. 205, pp. 352–373, 2018.

[21] J. J. M. de Jong, W. Klaassen, and P. J. C. Kuiper, "Monitoring of rain water storage in forests with satellite radar," *IEEE transactions on geoscience and remote sensing*, vol. 40, no. 2, pp. 338–347, 2002.

[22] F. Ulaby and M. Craig Dobson, *Handbook of Radar Scattering Statistics for Terrain*, Artech House Publishers, 1989.